Regular Article

PHYSICAL CHEMISTRY RESEARCH
Published by the
Iranian Chemical Society
www.physchemres.org
info@physchemres.org

Phys. Chem. Res., Vol. 5, No. 4, 659-679, December 2017
DOI: 10.22036/pcr.2017.83378.1371

Physical Chemistry Studies of Acid Dye Removal from Aqueous Media by Mesoporous Nano Composite: Adsorption Isotherm, Kinetic and Thermodynamic Studies

I. Akbartabar[a], M.E. Yazdanshenas[a], H.A. Tayebi[b,*] and N. Nasirizadeh[a]

[a]*Department of Textile Engineering, Yazd Branch, Islamic Azad University, Yazd, Iran*

[b]*Department of Textile Engineering, Qaemshahr Branch, Islamic Azad University, Qaemshahr, Iran*

(Received 27 April 2017, Accepted 2 July 2017)

In this research, SBA-15/Polypyrrole (SBA-15/PPy) mesoporous nanocomposite was synthesized, characterized and applied for Acid Blue 62 (AB62) adsorption as a textile dye from aqueous solution. In order to evaluate the structural properties of the synthesized adsorbent, FT-IR, FESEM and TEM images, XRD, and BET techniques were applied. Some parameters such as pH, dosage, and time which affect the batch adsorption process were investigated and optimized as well. The optimized condition was achieved by 0.3 g l^{-1} adsorbent at pH = 2 and 60 min in contact. In addition, Langmuir, Freundlich, Temkin, Dubinin-Radushkevich (D-R) and Redlich-Peterson (R-P) adsorption isotherms were employed to determine type of adsorption isotherm. The results showed the agreement of experimental data with Langmuir adsorption isotherm with maximum dye 1428.571 mg g^{-1} adsorption capacity. The kinetic analysis was carried out by pseudo-first-order, pseudo-second-order, intra-particle diffusion and Elovich models. The results revealed that the adsorption kinetic is more similar to the pseudo -second-order. The parameters of thermodynamic like ΔH°, ΔG° and ΔS° were calculated. The ΔG° and ΔH° negative values and ΔS° positive values (5.155 J mol^{-1} K^{-1}) illustrated that AB62 adsorption process is physi-sorption, spontaneous, exothermic and feasible.

Keywords: SBA-15, Acid Blue 62, Polypyrrole, Kinetic, Isotherm

INTRODUCTION

Dyes are widely used in several sources, such as textiles, printing, dyeing, dyestuff manufacturing, cosmetics, food processing, pharmaceutical, Paper, rubber, plastics and leather; and their discharge into water causes environmental pollution [1-3]. Upon development of dyeing process and industries, one of the main sources of pollution, and consequently a common problem for many countries, is dye wastewaters. The dye wastewaters can potentially cause mutagenic, high biotoxicity, and carcinogenic effects on the aquatic toxicity and mammals. Additionally, they can cause health problems like skin irritation, allergic dermatitis, and cancer in humans. As a result, organic dyes should be removed from wastewater before discharging into water in order to minimize the pollution risks produced by these sewages [1-4].

Some methods have been carried out for dye removal from dye wastewaters. A wide range of methods containing physical, chemical and biological techniques have been performed to reduce their impact on the environment as well. Although some chemical and biological methods such as ozonation [6], coagulation [7], flocculation [8], photocatalytic degradation [9], hypochlorite treatment [10], trickling filter [11], activated sludge [12], chemical precipitation [13], physical separation [14], biological degradation [15], aerobic/anaerobic digestion [16], advanced oxidation processes (AOPs) [17] and

*Corresponding author. E-mail: tayebi_h@yahoo.com

electrochemical [18] techniques are suitable in removing dyes; they require some special equipments and are usually energy intensive. In addition, these processes often generate large amounts of byproducts. Among all techniques studied, physical processes such as adsorption was found to be an efficient and economic process to remove dyes, and to control the bio-chemical oxygen demand as well. Moreover, this method is efficient due to its simplicity, convenience, reversibility and insensitivity to toxic substances. This process helps to transfer the species from the water sewage to a solid phase by maintaining the volume of sewage at a minimum amount [1-3]. To gain this purpose, a large amount of new materials were applied as adsorbents.

Recently, mesoporous structures have attracted researchers as a novel type of adsorbents for removing organic compounds such as dyes, phenolic compounds [18, 19], and heavy metals due to their unique features like the high specific surface and large and tunable pore channels. Common used types of mesoporous silica structures are SBA-1 [20], SBA-3 [21], SBA-15 [22], SBA-16 [23], MCM-41 [24], MCM-48 [25] and hexagonal mesoporous silica (HMS) [26].

The SBA-15, a family of highly arranged mesoporous silica compounds, has attracted the great interest (to be modified and functionalized) due to its large mesopore volume, high surface area, thicker pore walls (3.1-6.4 nm), high thermal, hydrothermal stability, tailorable large offered pores from 4.6-30 nm, and slim distribution of pore size in comparison to other mesoporous silica structures [27]. In addition, it reveals the presence of micropores that are in control into the pore boundaries and also intra-connectivity in the channels of adjacent mesopore by micropores and slim mesopores. This non-stop network helps diffusion into the whole SBA-15 porous structure during adsorbing process. Therefore, it is vital to discover SBA-15 designation and modification support for high dyes adsorption capacity, especially higher than room temperature, by functionalization of amine [27]. The amine group plays a key role in determining the medicated silica mesoporous adsorbents performance. Various amines have been tested including alkanolamines [28], amine-containing silanes such as 3-amino propyl trimethoxysilane [29], oligomeric amines such as polyethyleneimine (PEI) [30] and tetraethylenepentamine (TEPA) [31], and conductive electroactive polymeric compounds such as polypyrrole (PPy) [32] and polyaniline (PAni) [33].

In the last decade, PPy has gained so much attention for its proper functionality such as sufficient electrical conductivity, low-cost monomer, non-toxicity, formation of adhesive coating by different substrates, electrochemical properties, and their unique features to hybrid with inorganic mesoporous compounds as well. Among them, PPys have been widely provided as adsorbents due to sufficient environmental stability to water and oxygen, simple preparation and high adsorption capacities for important media in removing pollutants from water. This led to an increasing interest in selecting polymeric adsorbents [34-37]. The modification of as-prepared SBA-15 mesoporous with conducting polymers can remarkably increase the adsorption capacity. Although a wide investigation has been carried out about the SBA-15 in the metal ion adsorption [38], there is no systematic study about dyes adsorption by SBA-15 modified with different amine-containing compounds.

In this study, SBA-15 was synthesized, and then functionalized by polypyrrole. The produced material was used as an adsorbent for removal of Acid Blue 62 from aqueous media. The effects of various parameters including adsorbent dose, initial concentration of the aqueous phase, and pH of the solution were thoroughly studied. Then, the absorption studies of Acid Blue 62 such as isotherms, kinetics and thermodynamics sorption were performed on the produced absorbents.

EXPERIMENTAL

Materials

In order to carry out the experiment, Surfactant Pluronic P123 ($EO_{20}PO_{70}EO_{20}$, average MW ~5800) was purchased from Sigma-Aldrich Corporation. Tetraethyl orthosilicate (TEOS, reagent grade 98%), hydrochloric acid (HCl, 37%) and sodium hydroxide (99.9%), and $FeCl_3 \cdot 6H_2O$ were provided from Merck Corporation. Pyrrole (Py, 99%) was obtained from Merck and distilled under reduced pressure

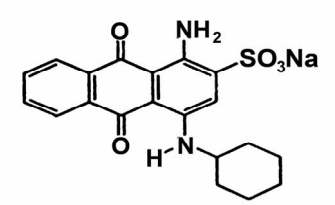

Fig. 1 Chemical structure of AB62.

Table 1. Characteristics of AB62

Name	CAS number	C.I. number	Formula	Molecular weight (g mol^{-1})	λ_{max} (nm)
Acid Blue 62	4368-56-3	62045	$C_{20}H_{19}N_2NaO_5S$	422.43	620

before using. Acid blue 62 (AB62), an anionic dye, (see Fig. 1 and Table 1) were obtained from Dystar. All chemicals were used without any further purification.

Nano-mesoporous Silica SBA-15 Preparation and Functionalization

In the present study, SBA-15 was prepared based upon the previous study [38]. Typically, 12.5 ml of P123 as amphiphilic block copolymer nonionic surfactant of the organic structure directing agent and 375 ml of distilled water along with 75 ml of HCl as the pH controlling agent were stirred at 42 °C. Next, we added 31.5 ml TEOS as a source of silica to the perfect mixture, and prepared gel was set in static conditions at temperature 42 °C for 24 h. Then, the hydrothermal temperature increased to 138 °C and kept for 24 h. Finally, after filtering process, we put gained powder for the calcination step at 550 °C for 5 h into a furnace for eliminating the organic compounds onto the pores.

Surface modifications over nano-mesoporous SBA-15 have been performed by post-synthesis grafting method. To modify the SBA-15 sorbents surface, 5.4 g of $FeCl_3$ was added into 100 ml of distilled water and stirred for 20 min. Next, SBA-15 (1 g) and 1 ml of pyrrole were added and mixed well for about 20 min, and then freshly distilled Pyrrole (1 ml) was added. The process was carried out at room temperature for 5 h. The obtained SBA-15/PPy nanocomposite filtered and rinsed with deionized water and acetone multiple times, then at 60 °C in an oven for 24 h was dried [39].

Instrumentation

SBA-15 surface morphology and SBA-15/PPy were observed by the field emission scanning electron microscopy (FESEM), TESCAN, and MIRA3 microscope. These nanomeso structure materials were characterized by transmission electron microscopy (TEM), Philips, CM/20, Netherlands. N_2 adsorption/desorption isotherms of the synthesized samples were performed by the Chem BET 3000 TPR/TDP tool, made in USA at 77 K to determine an average pore diameter. The specific surface area of nanomeso structures was measured by Brunauer-Emmet-Teller (BET). Pore diameters were recognized from the adsorption branch by Barrett-Joyner-Halenda (BJH). The total volume of pore was estimated using the adsorbed amounts under the relative pressure (P/P0). For analyzing the pristine meso structures, X-ray diffraction (XRD) in small-angle mode, patterns in the range $0.6 < 2\theta < 9$ were structurally cleared by XPERT-PRO40 kV spectrometer with radiation of Cu Kα ($\lambda = 1.5406$ Å). Fourier transform infra-red (FTIR) spectra obtained from the mesoporous SBA-15 and SBA-15/PPy were studied by Shimadzu model

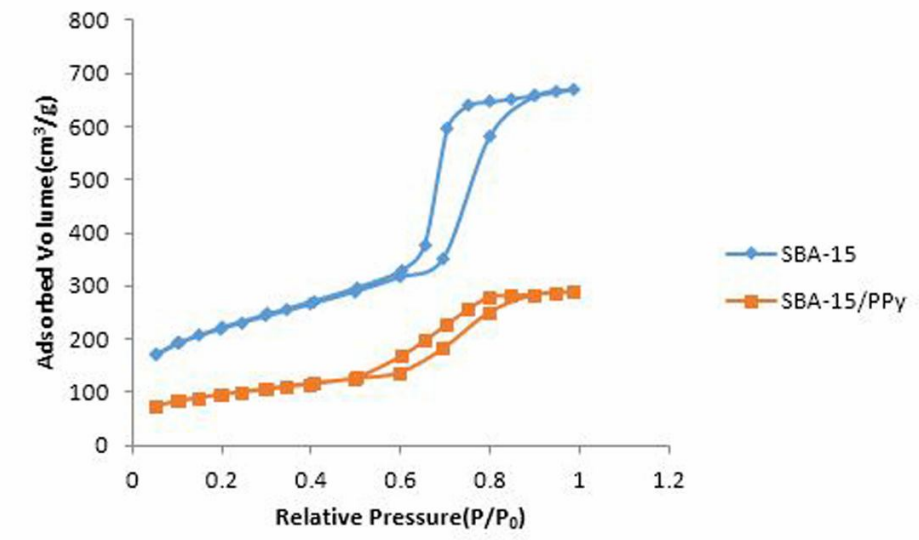

Fig. 2. N_2 adsorption/desorption isotherms of SBA-15 and SBA-15/PPy.

Table 2. Structural Properties of SBA-15 and SBA-15/PPy

Sample	Surface area (BET) ($m^2\ g^{-1}$)	Pore diameter (BJH) (nm)	Pore volume (BJH) ($cm^3\ g^{-1}$)
SBA-15	748.6	7.8	0.96
SBA-15/PPy	112.8	3.2	0.28

4300, Japan. The dyes adsorption was determined by UV-visible spectrophotometer Jenway, 6505, UK.

Adsorption Studies

All adsorption trials were performed in a 250 ml closed glass pyramid bottle using a shaker with 200 rpm. Batch experiments were conducted through mixing SBA-15 and SBA-15/PPy in different dosages with 100 ml AB62 solution with various concentrations at multiple pH values, temperatures and times. In order to adjust the pH values of the solution between 2 and 12, HCl and NaOH solutions with concentration of 0.1 M were used. In the last step, a centrifuge instrument (with 4000 rpm) was used to separate the adsorbent sample for 20 min. Also, the spectrophotometrically measurement of AB62 concentration in the solution was performed at 620 nm wavelength. Each experiment repeated five times and the experimental results bore average values. The percentage of removal efficiency of AB62 and equilibrium adsorbed amounts q_e (mg g^{-1}) were calculated by the following relationships:

$$R = \frac{(C_0 - C_e)}{C_0} \times 100 \quad (1)$$

$$q_e = \frac{(C_o - C_e)V}{W} \quad (2)$$

where C_0 and C_e are initial and equilibrium concentrations, in a row (mg l^{-1}) and V is dye bath volume (l) and W is adsorbent weight (g) .

The adsorbed amounts q_t (mg/g) were calculated using the following Eq. (3):

$$q_t = \frac{(C_o - C_t)V}{W} \quad (3)$$

where C0 and Ct represent dye concentrations at initial and different times, respectively (mg l^{-1}). V is the dye bath volume (l) and W is the adsorbent weight (g).

RESULTS AND DISCUSSION

Characterization

Specific surface area, mean size of pore diameter and, especially, pore size distribution of mesoporous materials were evaluated in this research. The SBA-15 and SBA15/PPy N_2 adsorption/desorption isotherms along with their B.J.H. pore size distributions are shown in Fig. 2 and Table 2. While SBA-15 represents sort IV IUPAC classical isotherm with a sort H1, we observed a sharp becoming more of taken N_2 at correct pressure P/P0 = 0.6 to 0.8 , demonstrating the formation of cylindrical pore channel as expected for mesoporous materials [38,40]. Also, this material not only has relatively high specific surface area, but also shows a narrow average pore size distribution at 7.8 nm. Regarding to SBA-15/PPy nanocomposite, the IV isotherm with a hysteresis loop is closed at P/P0 = 0.5. Also, the isotherm inflection point shifts to lower P/P0. Thus, SBA-15/PPy isotherm maintains the typical SBA-15 isotherm shape, but with the PPy contents. In addition, data reported in Table 2 indicate the falling in specific surface, SBA15/PPy mesopore volume and pore size that is included with the PPy grafting species on the silica surface at the molecular level, showing that well polymer agreement into SBA-15 channels has been achieved [38,40-42].

The merged SBA-15 internal morphology was investigated with TEM method (Fig. 3a). The electron beam was parallelly radiated on the main cylindrical pores axis. Also, the TEM image confirmed the well-organized hexagonal arrays of channels with high uniformity and pore diameter size, at 7-8 nm wavelengths, which are in agreement with the pore size calculated by BJH measurement method [38,41]. After being modified with PPy, the hexagonal meso-structure can be well retained (Fig. 3b), suggesting that the surface modification has not obviously destroyed the meso-structure. The results are consistent with the corresponding N_2 sorption results (Fig. 2).

Also, according to Fig. 4, the FESEM image depicts SBA-15 and SBA-15/PPy nanocomposite with a relatively uniform size in an almost hexagonal pillar. In addition, particulates polymerization agglomerates have shown some pores on the external and internal surface SBA-15, that states the assembly of small particle PPy. These results further illustrate that PPy has been successfully fixed on SBA-15 pore wall by this modification method.

synthesized SBA-15 XRD patterns and SBA-15/PPy samples (Fig. 5) show that three well-resolved diffraction peaks have been indexed, where the single strong peak (10 0) at 2θ = 0.95° related d spacing is 8.9 nm, and two less strong peaks are (110), (2 0 0) at 2θ = 1.59° and 1.81°, respectively, which represent a well-ordered silicate mesoporous structure with P6 mm hexagonal symmetry [43]. In this case, a small shift towards the larger diffraction angles, in comparison with the literature, can be due to the difference between the synthesis techniques and calcination temperatures [43-45].

Also, maintaining the ordered SBA-15/PPy nanocomposite meso-structure after PPy modification process, illustrated in Fig. 5, indicates the structure of materials which is remained unaltered after grafting amine functional group. However, the observed meaningful peak reduction force for SBA-15/PPy is relevant to filling SBA-15 pores with PPy polymers. Furthermore, XRD pattern includes thickness of silica walls, because the proximate SBA-15 pore size computed with BJH, 7.8 nm, is not bigger than d 8.9 nm for the XRD pattern peak (10 0) [38,41].

The FTIR spectroscopy provides the important information about the SBA-15/PPy nanocomposite formation. The FTIR spectra and analysis of SBA-15 and SBA-15/PPy nanocomposite, as shown in Fig. 6, confirms the SBA-15 formation based upon the characteristic peaks of silicate materials. The bands 788 and 1099 cm^{-1} belong to the symmetrical vibrations and asymmetric Si-O-Si bending of SiO_4 skeleton. The peaks at 466, 935 and 3434 cm^{-1} indicate the torsion vibration of the Si-O-Si bond and the Si-OH group, respectively. The appearances of characteristic peaks show the presence of Si-OH groups on the silica pore wall. After the surface modification, some new peaks and also some invisible peaks can be observable on the FTIR spectra of SBA-15/PPy (Fig. 6b). In addition, an exception

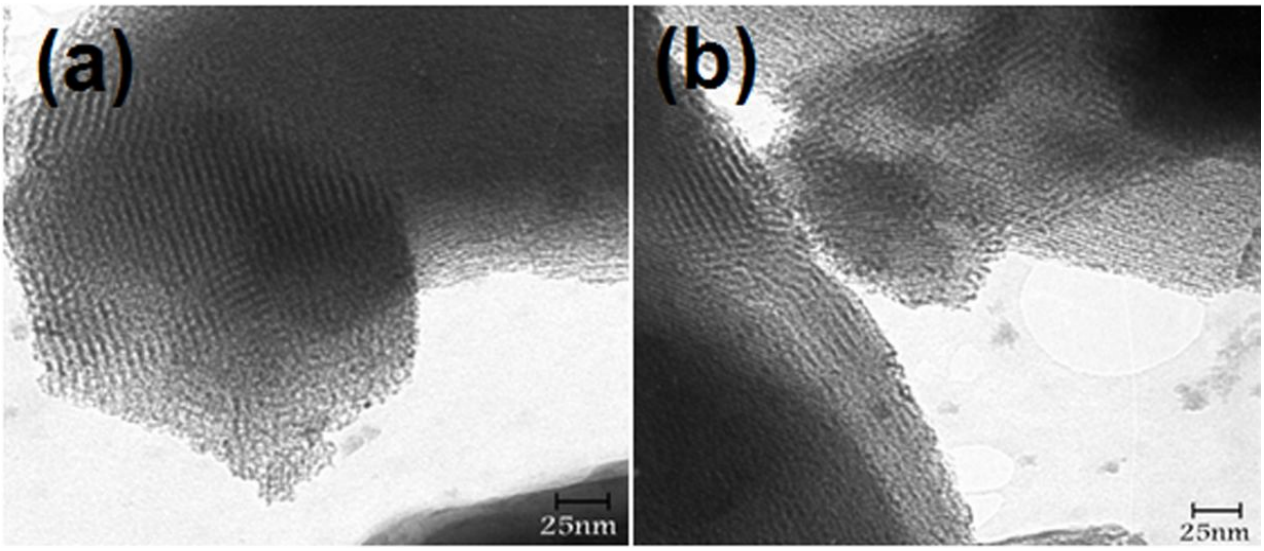

Fig. 3. TEM Morphology images of (a) SBA-15 and (b) SBA-15/PPy nanocomposite.

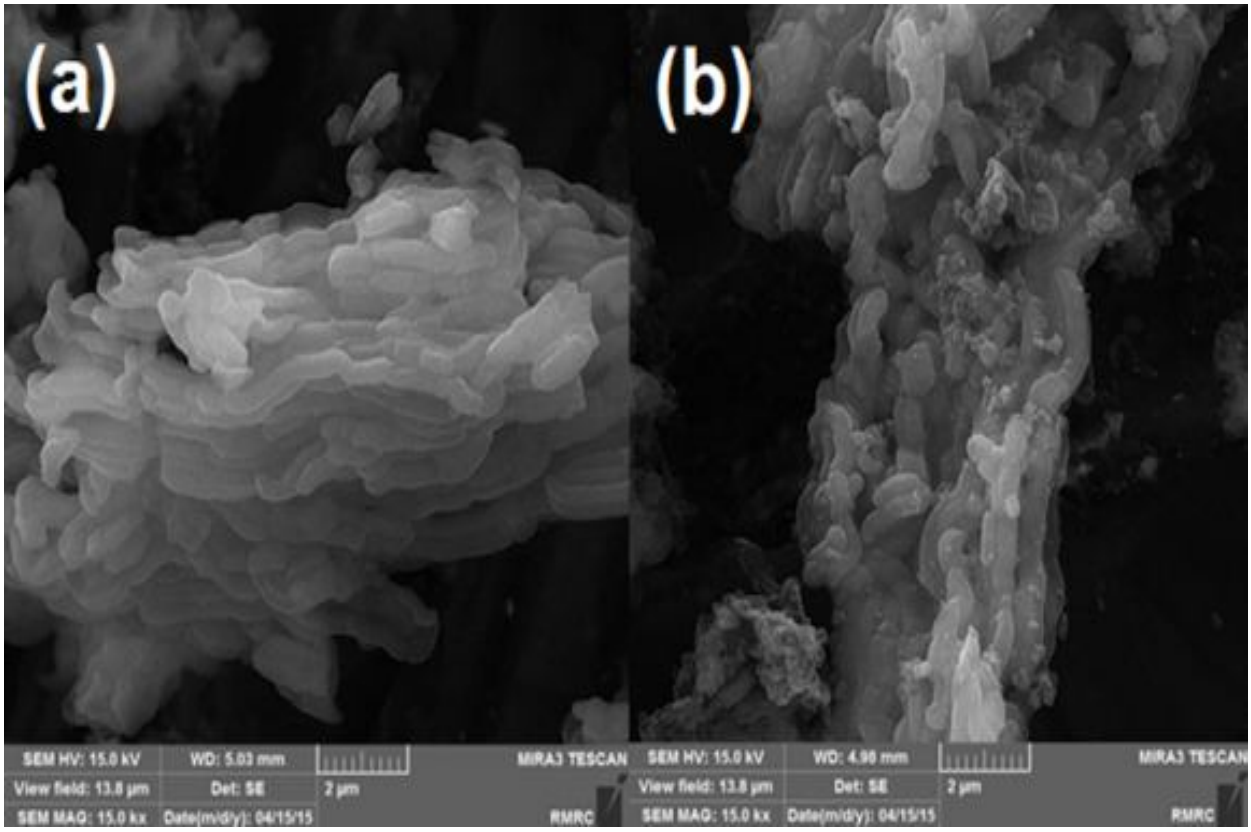

Fig. 4. FESEM Morphology images of (a) SBA-15 and (b) SBA-15/PPy nanocomposite.

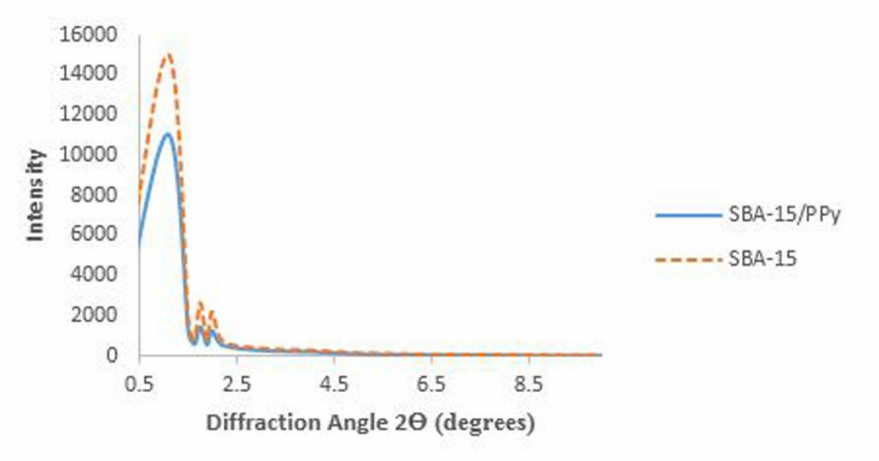

Fig. 5. XRD patterns of SBA-15 and SBA-15/PPy.

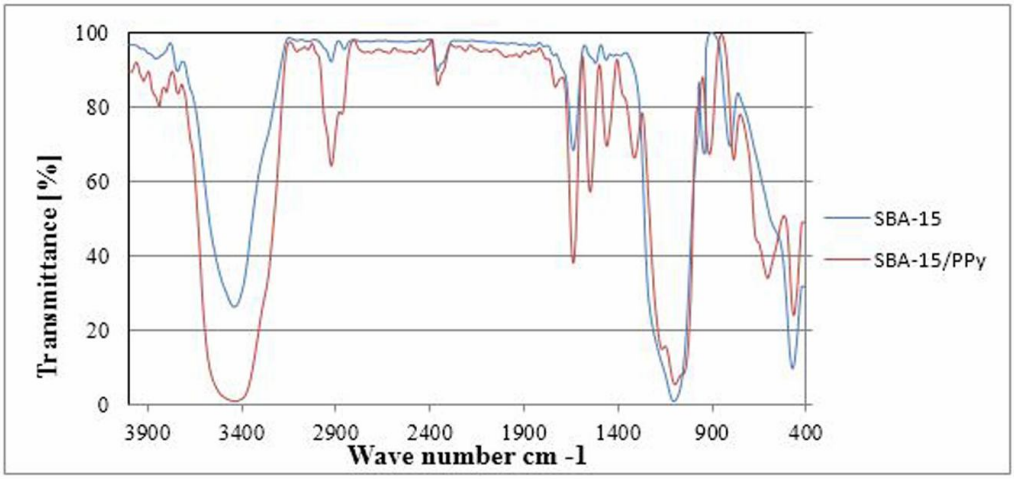

Fig. 6. FTIR spectra of SBA-15 and SBA-15/PPy.

of the peaks involved with SBA-15 silica indicates the incorporation between PPy polymer chains and SBA-15 materials [38,43].

The main characteristic peaks for SBA-15/PPy are assigned as follows: the strong broad band at 3427 cm^{-1} can be attributed to the single bridge compounds with polymeric association, the bands at 2918 and 2356 cm^{-1} refer to the stretching vibration of C-H and C-N stretching vibration, respectively, the C=C ring stretching of pyrrole and C-H vibrations was assigned at 1635 and 1305 cm^{-1}, respectively. Also, the peak at 1091 cm^{-1} corresponds to the deformation of O-H group and C-O symmetric stretching. The peak at 910 cm^{-1} could be assigned to the C-H deformation vibration in the CH=CH group. These obtained results state the successful functionalization of PPy on the pore wall of SBA-15 [38,41,43,46]. The results of BET, TEM, FESEM, and XRD methods confirm this functionalization as well.

Adsorption Studies

pH Effects. In this research, an important factor is the solution pH value which controls the dye adsorption from aqueous solution on the active sites of adsorbent surface [38]. Additionally, in the processing of adsorption the adsorbent surface charge is affected by pH values. Therefore, the dye adsorption aspect was studied with switching pH from 2 till 12, while other factors such as

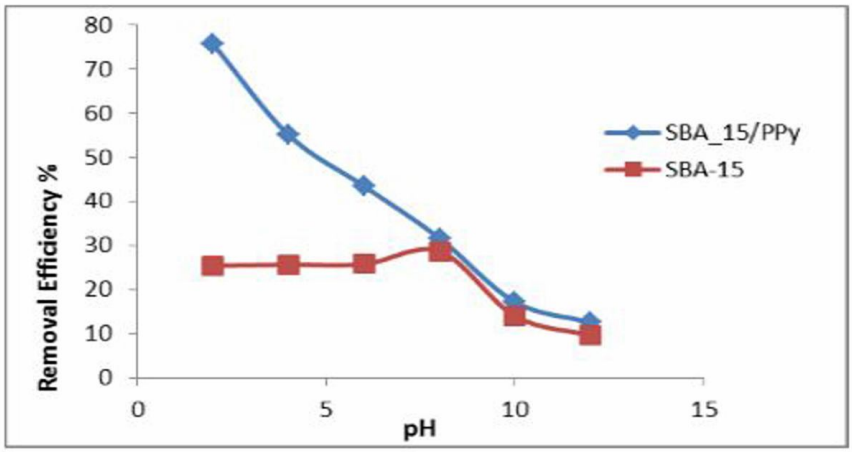

Fig. 7. Effect of pH on the removal efficiency with SBA-15/PPy and SBA-15(initial concentration = 40 mg l^{-1}, contact time = 120 min, adsorbent dosage = 0.2 g l^{-1}).

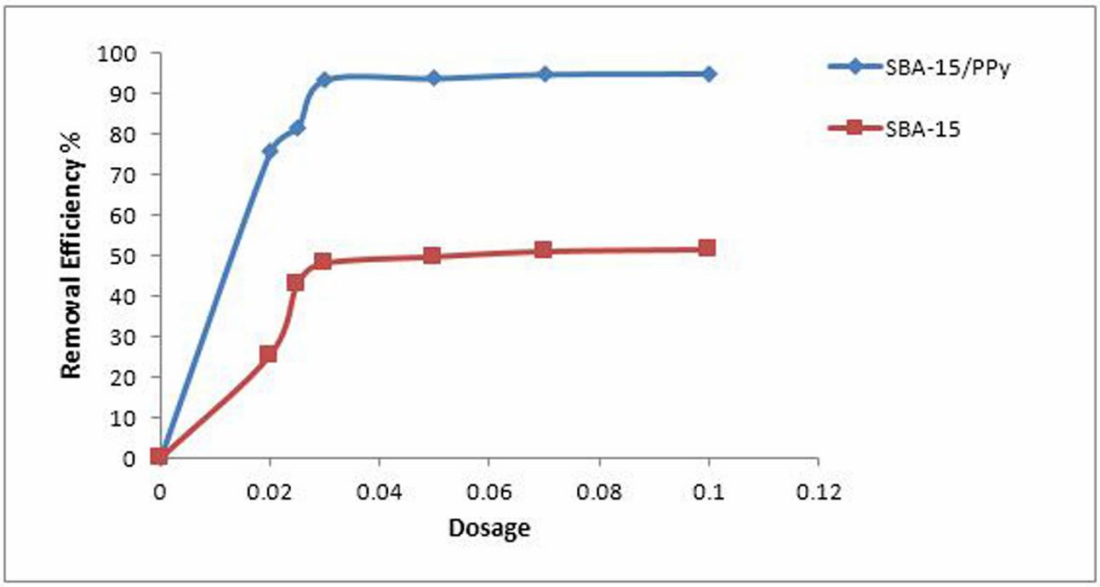

Fig. 8. Effect of adsorbent dosage on the removal efficiency with SBA-15/PPy and SBA-15 (initial concentration = 40 mg l^{-1}, contact time = 120 min, pH = 2).

adsorbent storage, dye concentration, time and temperature remained constant. The experiment was carried out by 40 mg l^{-1} initial concentration and 0.02 g adsorbent at room temperature and contact time of 120 min. The pH changes on removal efficiency of AB62 have been demonstrated in Fig. 7. It is stated that the most AB62 adsorption value is obtained at pH 2. According to Fig. 7, the dye adsorption increases with pH decreasing and an optimum rate is achieved at pH about 2 and removal 75.7% efficiency. At lower pH, it may lead to adsorbent surface protonation, [38] because for anionic dye adsorption (AB62) by the adsorbent, the adsorbent must have a positive charge. In

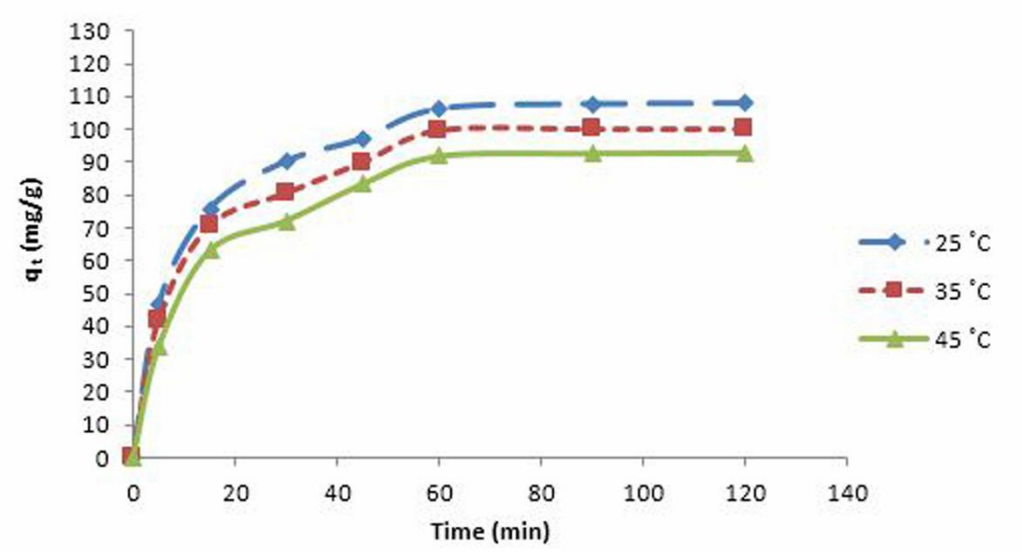

Fig. 9. Effect of contact time and temperature on the amount of AB62 dye adsorption on SBA-15/PPy (initial concentration = 40 mg l^{-1}, adsorbent dosage = 0.3 g l^{-1}, pH = 2).

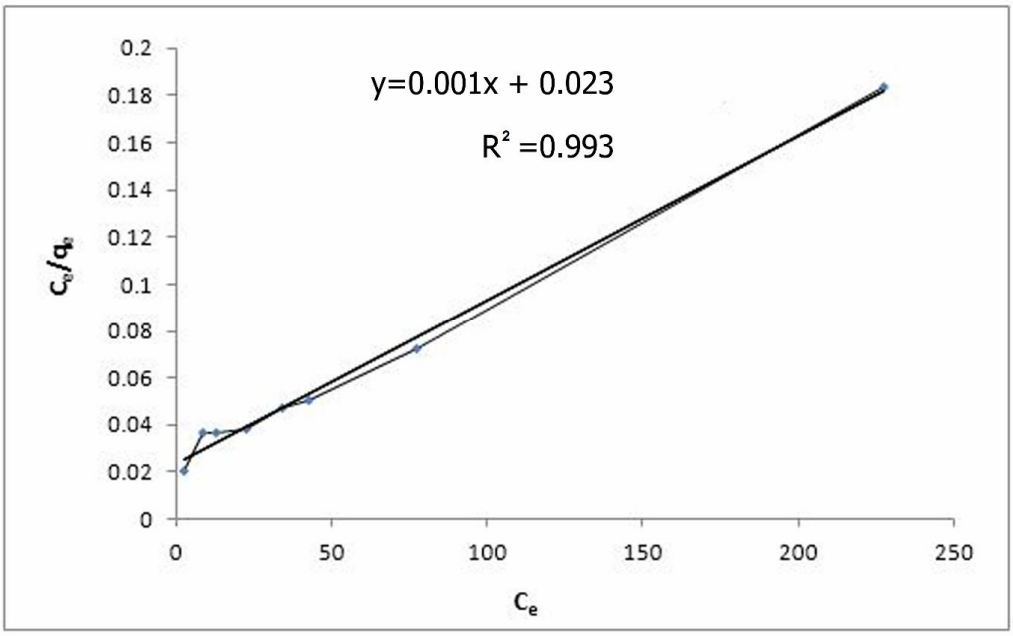

Fig. 10. Langmuir adsorption isotherm for the adsorption AB62 onto SBA-15/PPy.

acid situations, the amino PPy ($-NH_2$) bands are protonated in the existence of obtained H^+ protons; so, with adsorption surface protonation, the tendency of AB62 to the adsorption surface increases [38,39].

SBA-15/PPy nanocomposite adsorbs more dyes, since the hydroxyl groups on the surface of pure silica is not able

to create strong interactions with acid dyes [3]. In fact, the functionalization of mesoporous silica with amine groups enhances the adsorption capacity. Actually, the higher SBA-15/PPy adsorption capacity may be due to the processing by electrostatic interaction and hydrogen bond formation between adsorbent surface and acid dyes [3].

Adsorbent Dosage Effect

The adsorbent dosage plays an important role in determining removal efficiency and adsorption capacity. The effect of adsorbent amounts (SBA-15 and SBA-15/PPy) on the acid dye adsorption was evaluated by the weight range from 0.02 to 0.10 g and 100 ml solution of 40 mg l^{-1} AB62 at pH 2. Results are shown in Fig. 8. Getting high adsorbent to 0.1 grams increases the adsorption sites and consequently the removal efficiency as expected. At 0.1 g, highest efficiency is about 95.06%. Although, adsorbent dose increases to more than 0.03 g, it does not change eliminating efficiency, which might be attributed to the aggregation of adsorbent particles, decreasing the surface area and less adsorption sites availabe [3,39]. In addition, the amounts of adsorbent might affect the physical properties of the solid-liquid suspensions by some factors such as inhibiting the dye molecules to diffuse onto the adsorbent surface and increasing the viscosity [47]. Therefore, 0.3 g l^{-1} nanocomposite is considered as suitable adsorbent for AB62 elimination in this study.

Contact time effect. Determining the equilibrium time is one of the most vital characteristics showing the dye adsorption on adsorbent. According to Fig. 9, the adsorption of AB62 by SBA-15/PPy adsorbent for different periods of contact time (5-120 min) and temperatures (25, 35 and 45 °C) was investigated. 40 mg l^{-1} initial dye concentration, pH = 2, and 0.03 g adsorbent dosage in 100 ml were employed. It is clear that in primal adsorption stage (until 15 min), AB62 elimination has a higher rate because of more accessibility of active sites, and then consequently continues at a lower rate until the equilibrium is gained at 60 min, when adsorption sites become complete. This means that the longer time has no influence on dye adsorption. As a matter of fact, the optimum 60 min contact time was chosen for the next tests.

As shown in Fig. 9, adsorbate amount per adsorbent unit mass at time t, (q_t,) is decreased with temperature increasing from 25 to 45 °C. Therefore, AB62 adsorption process on SBA-15/PPy nanocomposite is exothermic nature.

Adsorption Isotherm

The adsorption equilibrium is one of the most significant physicochemical aspects in evaluating adsorption process [3]. The adsorption isotherm indicates adsorbent interaction with adsorbate, and this research needs to design the adsorption systems for removing dyes. These adsorption isotherms can successfully be applied for scaling-up batch type processes. For surveying AB62 adsorption, lab studies were analyzed by 0.03 g SBA-15/PPy adsorbent at suitable pH 2 and 25 °C. In this study, five isotherm models were examined for the equilibrium adsorption data treatments. These isotherms including Langmuir, Freundlich, Temkin, Dubinin-Radushkevich (D-R) and Redlich-Peterson(R-P) models were selected to explore AB62 adsorption in our study.

The Langmuir isotherm model supposes a monolayer adsorption with adsorption sites and energies which are in homogeneous distribution, without interactions among adsorbed dye molecules [48]. In the case of Freundlich model, an empirical equation struggles with physic-chemical adsorption on heterogeneous layer at sites with different adsorption energy and with non-identical adsorption sites that are not always reachable [39] and it is not restricted to the monolayer adsorption pattern. Also, this isotherm considers that the sites with stronger affinity are occupied first [3]. Temkin isotherm model, with no focusing on extremely low and high amount of concentrations, supposes that due to interactions, all molecules heat adsorption in the layer would decrease linearly rather than logarithmically with cover [49,50]. The Eqs. (4), (5) and (6) represent the linear form of the Langmuir, Freundlich and Temkin isotherms, respectively:

$$\frac{C_e}{q_e} = \frac{C_e}{q_m} + \frac{1}{bq_m} \tag{4}$$

$$\ln q_e = \ln K_f + 1/n \ln C_e \tag{5}$$

$$q_e = K_1 \ln(C_e) + K_1 \ln(K_2) \tag{6}$$

where q_e is the adsorbent equilibrium capacity of adsorption

Table 3. Isotherm Parameters for the Adsorption of AB62 onto SBA-15/PPy

			Langmuir
q_m (mg g^{-1})	b (l mg^{-1})		R^2
1428.571	0.029		0.993
			Freundlich
K_f (mg g^{-1})/(mg $l^{-1})^{1/n}$	n		R^2
84.690	1.788		0.932
			Temkin
K_1 (J mol^{-1})	K_2 (l g^{-1})		R^2
282.5	0.394		0.95
Redlich–Peterson			
K_R (l mg^{-1})	α_R (l mg^{-1})	β	R^2
62.5	0.177	0.071	0.946
Dubinin–Radushkevich			
q_S (mg g^{-1})	E (kJ mol^{-1})		R^2
677.9	408.163		0.619

(mg g^{-1}) , C_e is the equilibrium concentration (mg l^{-1}), q_m is the highest monolayer adsorption capacity (mg g^{-1}), b is the Langmuir constant related to the adsorption energy (l/mg), K_f is the adsorbent adsorption capacity and n is the empirical constant for adsorption intensity. In process of adsorbing, the high rates of n are suitable. Also, K_2 is the equilibrium binding constant, related to the highest binding energy, and K_1 is related to the heating of adsorption [50]. b and q_m of Langmuir obtained from plotted C_e/q_e *vs*. C_e data (Fig. 10) and K_f and n for Freundlich from plotted lnq_e *vs*. lnC_e data and K_1 and K_2 for Temkin from plotted q_e versus lnC_e data were estimated for AB62 adsorption on SBA-15/PPy, and the corresponding values are reported in Table 3.

Another well-known used equation in the high degree of rectangular isotherms analysis is D-R isotherm model [51], generally was utilized to state the mechanism of adsorption with a Gaussian energy distribution into a heterogeneous surface. This model is often successfully fitted with the intermediate range of data concentrations and high solute activities [50] in which the linear equation is as follows:

$$\ln(q_e) = \ln(q_s) - B\varepsilon^2 \quad (7)$$

where q_s is D-R constant and ε can be calculated by:

$$\varepsilon = RT\ln\left[1+\frac{1}{C_e}\right] \quad (8)$$

where B is denoted as the isotherm constant. The approach is usually used to specify the physicochemical adsorption dye, with its average free energy (E) sorption per adsorbate molecule, when it is moved to the solid surface from initial solution infinity and can be calculated by:

Table 4. A comparison between the Results of the Present Work and some Reported Results in the Literature

Sorbent material	Dye	Adsorption capacity ($mg\ g^{-1}$)	Isotherm model	Ref.
SBA-3/PEHA	Acid yellow 127	1250	Freundlich	[3]
	Acid red 114	1000	Freundlich	
	Acid blue 113	769.23	Freundlich	
NH_3^+-MCM-41	Acid fuchsine (Acid violet 19)	251.76	Langmuir	[4]
SBA-3	methyl orange (Acid orange 52)	357.1	Freundlich	[5]
	orange G (Acid orange 10)	434.7	Freundlich	
Chitosan	Acid orange 10	922.9	Langmuir	[54]
	Acid orange 12	973.3	Langmuir	
	Acid red 18	693.2	Langmuir	
	Acid red 73	728.2	Langmuir	
	Acid green 25	645.1	Langmuir	
Activated carbon	Acid Blue 80	171.028	Langmuir	[55]
	Acid red 114	103.75		
	Acid yellow 117	185.712		
Activated carbon (Waste bagasse by $ZnCl_2$)	Acid orange 10	4.86	Langmuir	[56]
Orange peel	Acid violet 17	19.88	Langmuir	[57]
Activated carbon (high ash raw bagasse by CO_2)	Acid blue 80	391	Langmuir Freundlich	[58]
Activated palm ash	Acid green 25	181.8	Freundlich	[59]
Magnetic $ZnFe_2O_4$ nanoparticles	Acid red 88	111.1	Langmuir	[60]
Natural clay	Acid red 88	1133.1	Langmuir	[61]
Na-bentonite	Acid blue 193	67.1	Freundlich	[62]
DTMA-bentonite		740.5	Langmuir	
Soy meal hull	Acid blue 92	114.94	BET	[63]
	Acid red 14	109.89	Freundlich	
SBA-15/PPy	Acid blue 62	1428.571	Langmuir	This work

$$E = \left[\frac{1}{\sqrt{2B}} \right] \quad (9)$$

Where R and T are the gas constant (8.314 J mol^{-1} K^{-1}) and absolute temperature (K), respectively. In the D-R isotherm, a plot of $\ln q_e$ *vs.* ε^2 indicates q_s and E constants (Table 3). All the coefficients, R^2, and constants used for five isotherms in this study are summarized in Table 3.

The R-P isotherm model is a combination of both Langmuir and Freundlich isotherms, which incorporates three parameters into an empirical equation. It approaches the high concentrations in the Freundlich model and is in agreement with the low concentration limitation in the Langmuir model. The model designated a three-parameter equation, which may represent adsorption equilibriums over an expanded concentration range; therefore, it can be utilized either in homogeneous or heterogeneous systems because of its high versatility [50,52]. It can be stated as the equation which follows:

$$q_e = \frac{K_R C_e}{1 + \alpha_R C_e^{\beta}} \quad (10)$$

where K_R, a_R, and β are R-P isotherm (l g^{-1}), R-P isotherm (l mg^{-1}), and the exponent constants lying between 0 and 1, respectively. If β = 1, Langmuir is better isotherm whereas the Freundlich isotherm can be the suitable isotherm if β = 0. However, the equation will not be linearized for easy isotherm parameter estimations. The expression linearization gives

$$\ln\left[\frac{K_R C_e}{q_e} - 1 \right] = \ln \alpha_R + \beta \ln C_e \quad (11)$$

Plotting Eq. (11) cannot be applicable since it contains three unknown parameters, a_R, K_R and β. Therefore, a minimization is used to solve the equations by maximizing the correlation coefficient between theoretical data from Eq. (11) and experimental data [53].

In Table 3, we see the isotherm models that have been plotted for adsorption data at 25 °C with calculated and shown model parameters. As shown, the Langmuir model's output data is more appropriate than other models. Moreover, it can be seen from Table 3 that the values of correlation coefficients are much higher than other four isotherms. In all cases, the D-R equation represents the poorer experimental data fit than the others.

The adsorption results of dye reported in the literature by different sorbent materials are represented in Table 4. As seen in this table, the maximum adsorption capacity of SBA-15/PPy obtained for dye in this study is comparable, that was 1428.571 mg g^{-1} and was found to be higher than other sorbent materials. The higher adsorption capacity of the adsorbent used in this study may be get from properties of SBA-15/PPy.

Adsorption Kinetics

Adsorption kinetics, indicating the absorption rate, is an important characteristic of adsorbents. A limiting step in the adsorption process is to find a desired mechanism such as chemical reaction and mass transfer [53]. Different kinetic models have been applied for evaluating experimental data. In this part, for investigating the kinetics process of AB62 adsorption on SBA-15/PPy nanocomposite, four kinetic models consisting pseudo-first-order, pseudo-second-order, intra-particle diffusion equation and Elovich model were utilized. In general, for fitting the kinetic data, the pseudo-first and -second models of linear kinetic are illustrated *via* Eqs. number (12) and (13);

$$\ln(q_e - q_t) = \ln q_e - tk_1 \quad (12)$$

$$\frac{t}{q_t} = \frac{1}{k_e q_e^2} + \frac{t}{q_e} \quad (13)$$

where k_1 and k_2 are pseudo-first order and pseudo-second order rate constants, respectively; q_e and q_t are the adsorbate amount per unit of adsorbent at equilibrium and time t (mg g^{-1}), respectively. Constants of rate and equilibrium adsorption capacities for pseudo-first-order and pseudo-second-order were estimated from the plot of $\ln(q_e - q_t)$ *vs.* t and plot of t/q_t *vs.* t (Fig. 11), respectively and the corresponding values are reported in Table 5. Moreover, the high value of correlation coefficient shows that this model can be used to describe adsorption kinetics.

To find the desired procedure and also rate-controlling steps which affect adsorption kinetics, the kinetic

Table 5. Kinetic Parameters for the Adsorption of AB62 onto SBA-15/PPy

Pseudo-first-order	K_1 (min^{-1})	q_e (mg g^{-1})	R^2
	0.052	71.593	0.993
Pseudo-second-order	K_2 (min^{-1})	q_e (mg g^{-1})	R^2
	0.0013	142.857	0.999
Intraparticle diffusion	K_{id} (mg g^{-1} min^{-1})		R^2
	6.681		0.814
Elovich	α (mg g^{-1} min^{-1})	β (mg g^{-1})	R^2
	68.281	0.050	0.949

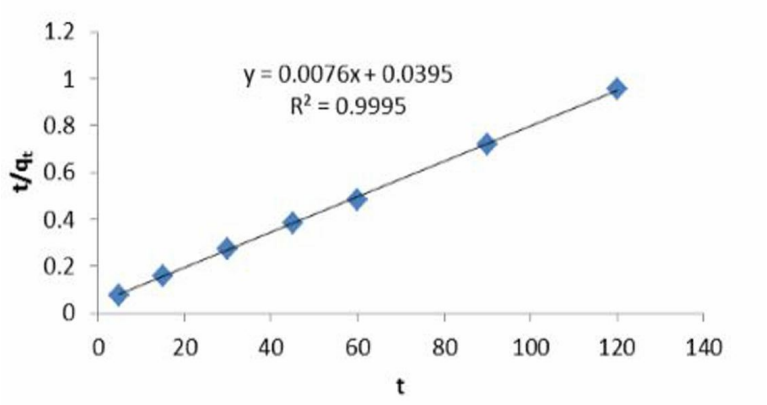

Fig. 11. Pseudo-second-order adsorption kinetic for the adsorption AB62 onto SBA-15/PPy.

experimental consequences were used in the intra-particle diffusion [52,53]. The limiting-step rate might be single or steps of diffusion mixture. Generally adsorption process is that the uptake varies almost proportionally with $t^{1/2}$, the Weber-Morris plot, compared to the contact time, t [52], whose model is expressed as:

$$q_t = K_{id}\, t^{1/2} + C \qquad (14)$$

where C is the intercept and K_{id} is the intra-particle diffusion rate constant, (mg g^{-1} $min^{-1/2}$), which can be appraised from the slope of the linear plot of q_t *vs.* $t^{(1/2)}$ as shown in Fig. 12, for predicting the step of rate limiting. From Fig. 12, it is stated that the adsorption of AB62 includes a few linear plots. Due to the diffusion of boundary layer and central deviation, the first part of the plot states the thickness of boundary layer. In the next diagram part, the reduction of adsorption depicts the diffusion of inside-particle in the process [53]. This confirms that the intra-particle diffusion cannot be only a rate-controlling step. For diffusion of inside-particle model, the appraised rate constant K_{id} and R^2, by regression of data, are 6.681 and 0.814, respectively.

One of the most useful models for describing such activated chemical adsorption is the Elovich kinetic model, which is expressed as follows:

$$q_t = 1/\beta \ln(\alpha\beta) + 1/\beta \ln t \qquad (15)$$

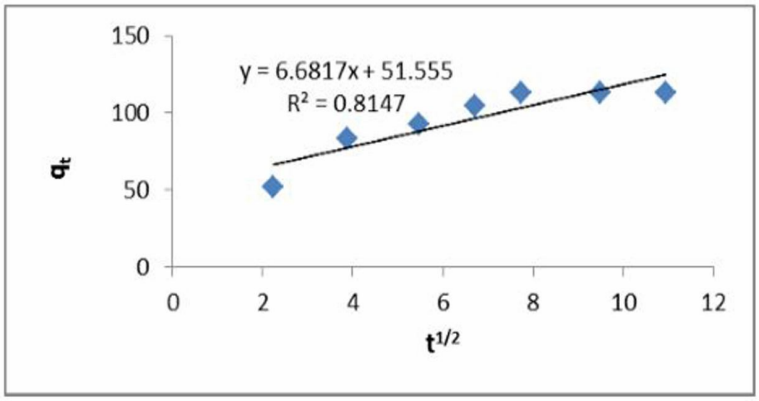

Fig. 12. Intra-particle diffusion adsorption kinetic for the adsorption AB62 onto SBA-15/PPy.

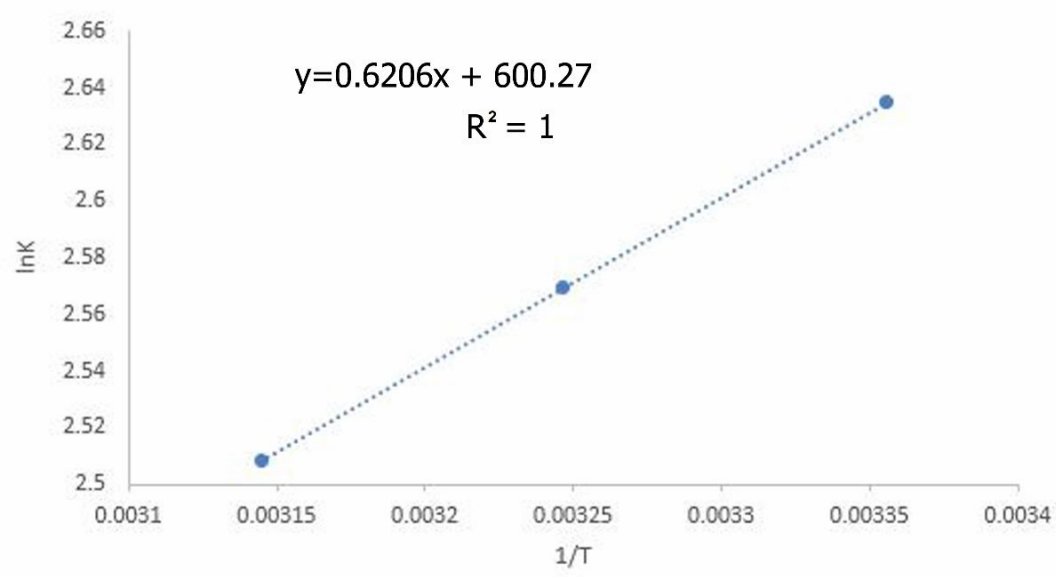

Fig. 13. Van't Hoff Regression for the adsorption AB62 onto SBA-15/PPy.

where q_t is the adsorption capacity at time t (mg g^{-1}), α is the initial adsorption rate (mg g^{-1} min^{-1}) and β is the desorption constant (gm g^{-1}) during each experiment. Therefore, the constants can be achieved by the slope and intercept of a straight line in the plot of qt *vs*. ln(t). Table 5 shows Elovich model constant, in which with high α and low β value, the adsorption rate increases.

Table 5 represents the correlation coefficients (R^2) of four kinetics models. The counted correlation coefficients are closer to unity pseudo-second-order kinetics model than the others. Consequently, the AB62 adsorption kinetic on SBA-15/PPy is in agreement with the pseudo-second-order reaction.

Adsorption Thermodynamics

To find out the inherent energetic changes and the adsorption mechanism, the thermodynamic analysis has been performed. Also, to estimate the effects of temperature on the AB62 adsorption by SBA-15/PPy and predict the adsorption thermodynamic behavior, Gibbs free energy

Table 6. Thermodynamic Parameters for the Adsorption of AB62 onto SBA-15/PPy

T (°C)	K_d (l mol^{-1})	ΔG° (kJ mol^{-1})	ΔH° (kJ mol^{-1})	ΔS° (J mol^{-1} K^{-1})	R^2
25	13.943	-6.528			
35	13.059	-6.579	- 4.990	5.155	1
45	12.284	-6.631			

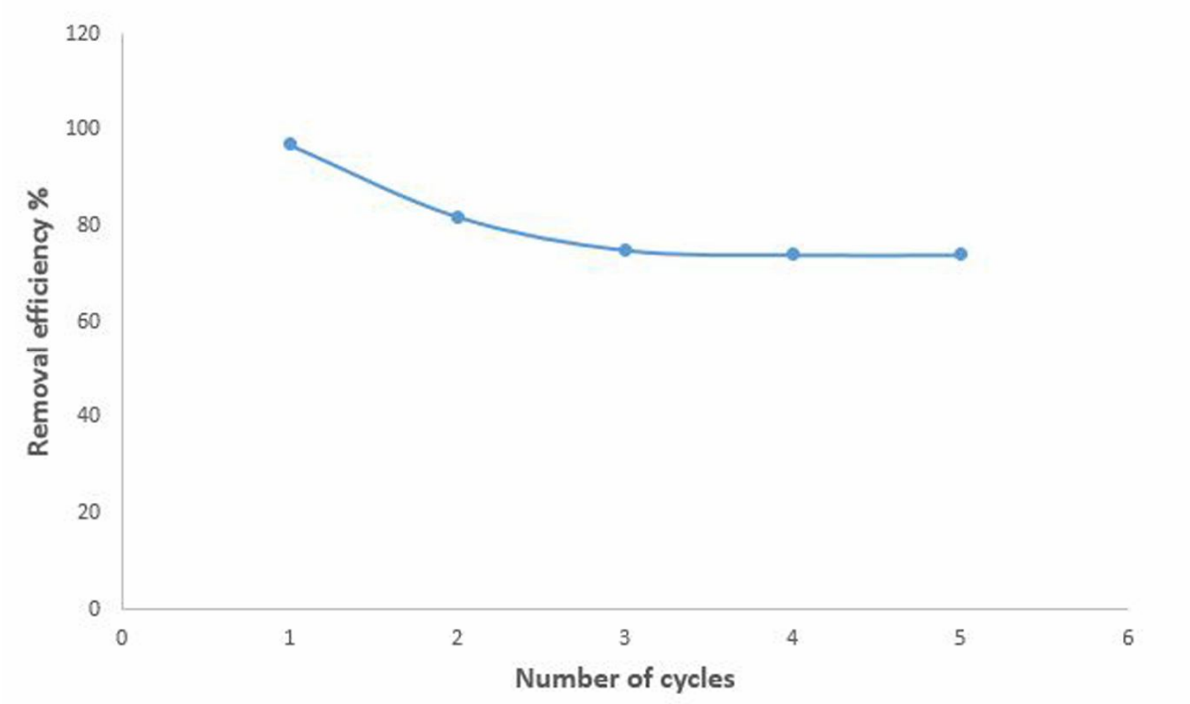

Fig. 14. Regeneration studies of SBA-15/PPy. (Initial Concentration: 40 mg l^{-1}, contact time: 120 min, temperature: 25 °C, pH: 2, dosage: 0.2 g l^{-1}).

(ΔG°), enthalpy (ΔH°), and entropy (ΔS°) amounts are calculated *via* Eqs. (16) and (17) as follows:

$$\Delta G = -RT\ln K_d \quad (16)$$

$$\ln K = \frac{\Delta S}{R} - \frac{\Delta H}{RT} \quad (17)$$

where K_d is the partition ratio. ΔH (J mol) and ΔS (J mol^{-1} K^{-1}) are calculated by the slope and intercept of straight line in the plot of ln(K_d) *vs.* 1/T, as illustrated in Fig. 13.

The thermodynamic parameters are expressed in Table 6. The negative ΔG° values confirm the spontaneous and thermodynamically favorable characteristic of AB62 adsorption. Also, the values of ΔG° in the range of -20 to 0 kJ mol^{-1} demonstrate the AB62 adsorption in a physi-sorption process [51-53]. In addition, negative value of ΔH° in the AB62 adsorption shows its exothermic. Thus, a higher adsorption capacity was achieved at lower temperature [51-53]. The positive value of ΔS° represents

the reversible AB62 adsorption by SBA-15/PPy nanocomposite.

Adsorption and Desorption Studies

The desorption studies were carried out using 1 M NaOH solution. Results showed 15% drop in the adsorption capacity after first regeneration cycle (Fig. 14). This decrease in adsorption capacity might be caused due to the decomposition or damage caused by alkaline solution to certain functional groups present over the surface of SBA-15/PPy. The decrease in the adsorption capacity was about 7% for the second and third cycle. The removal efficiency remains almost constant (75%) for the consecutive cycles (up to three cycles) showing that the adsorbent could be used again and again without any further lost in adsorption capacity.

CONCLUSIONS

In this research, SBA-15/PPy mesoporous nanocomposite was synthesized. The results of the TEM images and N_2 adsorption/desorption demonstrate the formation of cylindrical pores and a well-organized hexagonal array of SBA-15 including the average 7-8 nm pore size and also high specific area. Also, the results of the FESEM and TEM images, XRD, FTIR and N_2 adsorption/desorption show the successful functionalization of PPy on the SBA-15 pore wall. The SBA-15/PPy nanocomposite is a suitable adsorbent for AB62 dye elimination of water. The highest removal was obtained by 0.03 g adsorbent in the 60 min contact time, 25 °C, and pH = 2. The experimental data was in a perfect agreement with the Langmuir isotherm. The highest adsorption ability of SBA-15/PPy nanocomposite (1428.571 mg g^{-1}) was achieved by Langmuir model. In addition, adsorption kinetic results illustrated that AB62 dye adsorption follows a pseudo second-order model. Moreover, according to the results achieved *via* parameters of thermodynamic such as entropy (ΔS°), enthalpy (ΔH°), and Gibbs free energy changes (ΔG°), it should be mentioned that adsorption mechanism was physi-sorption, exothermic, appropriate, spontaneous and feasible.

ACKNOWLEDGMENTS

The authors wish to thank Yazd Branch, Islamic Azad University and Qaemshahr Branch, Islamic Azad University for support of the project.

REFERENCE

[1] Zareyee, D.; Tayebi, H.; Javadi, S. H., Preparation of polyaniline/activated carbon composite for removal of reactive red 198 from aqueous solution. *Iran. J. Org. Chem.* **2012**, *4*, 799-802.

[2] Gan, Y.; Tian, Na.; Tian, X.; Ma, L.; Wang, W.; Yang, C.; Zhou, Z.; Wang, Y., Adsorption behavior of methylene blue on amine-functionalized ordered mesoporous alumina. *J. Porous Mater.* **2015**, *22*, 147-155, DOI: 10.1007/s10934-014-9881-9.

[3] Anbia, M.; Salehi, S., Removal of acid dyes from aqueous media by adsorption onto amino-functionalized nanoporous silica SBA-3. *Dyes Pigm.* **2012**, *94*, 1-9, DOI: 10.1016/j.dyepig.2011.10.016.

[4] Qin, Q.; Ma, J.; Liu, K., Adsorption of anionic dyes on ammonium-functionalized MCM-41. *J. Hazard. Mater.* **2009**, *162*, 133-139, DOI: 10.1016/ j.jhazmat.2008.05.016.

[5] Muthukumar, M.; Sargunamani, D.; Selvakumar, N.; Rao, J. V., Optimisatio of ozone treatment for colour and COD removal of acid dye effluent using central composite design experiment. *Dyes Pigm.* **2004**, *63*, 127-134, DOI: 10.1016/j.dyepig.2004.02.003.

[6] Shi, B.; Li, G.; Wang, D.; Feng, C.; Tang, H., Removal of direct dyes by coagulation: the performance of preformed polymeric aluminum species. *J. Hazard. Mater.* **2007**, *143*, 567-574, DOI: 10.1016/j.jhazmat.2006.09.076.

[7] Riera-Torres, M.; Gutiérrez-Bouzán, C.; Crespi, M., Combination of coagulation-flocculation and nanofiltration techniques for dye removal and water reuse in textile effluents. *Desalination* **2010**, *252*, 53-59, DOI: 10.1016/j.desal.2009.11.002.

[8] Gupta, V. K.; Jain, R.; Nayak, A.; Agarwal, S. H.;

Shrivastava, M., Removal of the hazardous dye-tartrazine by photodegradation on titanium dioxide surface. *Mater. Sci. Eng., C* **2011**, *31*, 1062-1067, DOI: 10.1016/j.msec.2011.03.006.

[9] Yang, C. H.; Lee, C. C.; Wen, T. C., Hypochlorite generation on Ru-Pt binary oxide for treatment of dye wastewater. *J. Appl. Electrochem.* **2000**, *30*, 1043-1051, DOI: 10.1023/A: 1004038503410.

[10] Kornaros, M.; Lyberatos, G., Biological treatment of wastewaters from a dye manufacturing company using a trickling filter. *J. Hazard. Mater.* **2006**, *136*, 95-102, DOI: 10.1016/j.jhazmat.2005.11.018.

[11] Chu, H. C.; Chen, K. M., Reuse of activated sludge biomass: I. removal of basic dyes from wastewater by biomass. *Process Biochem.* **2002**, *37*, 595-600, DOI: 10.1016/S0032-9592 (01)00234-5.

[12] Zhu, M.; Lee, L.; Wang, H.; Wang, Z., Removal of an anionic dye by adsorption/precipitation processes using alkaline white mud. *J. Hazard. Mater.* **2007**, *149*, 735-741, DOI: 10.1016/j.jhazmat.2007.04.037.

[13] Ai, L.; Zhou, Y.; Jiang, J., Removal of methylene blue from aqueous solution by montmorillonite/$CoFe_2O_4$ composite with magnetic separation performance. *Desalination* **2011**, *266*, 72-77, DOI: 10.1016/j.desal.2010.08.004.

[14] Daneshvar, N.; Khataee, A. R.; Rasoulifard, M. H.; Pourhassan, M., Biodegradation of dye solution containing malachite green: Optimization of effective parameters using taguchi method. J. Hazard. Mater. **2007**, 143, 214-219, DOI: 10.1016/j.jhazmat.2006.09.016.

[15] Sponza, D. T.; Isik, M., Decolorization and azo dye degradation by anaerobic/aerobic sequential Process. *Enzyme Microb. Technol.* **2002**, *31*, 102-110, DOI: 10.1016/S0141-0229 (02)00081-9.

[16] Shu, H.; Huang, C.; Chang, M., Decolorization of mono-azo dyes in wastewater by advanced Oxidation process: A case study of acid red 1 and acid yellow 23. *Chemosphere* **1994**, *29*, 2597-2607, DOI: 10.1016/0045-6535(94)90060-4.

[17] Vlyssides, A. G.; Papaioannou, D.; Loizidoy, M.; Karlis, P. K.; Zorpas, A. A., Testing an electrochemical method for treatment of textile dye wastewater. *Waste Manage.* **2000**, *20*, 569-574, DOI: 10.1016/S0956-053X(00)00028-3.

[18] Shukla, P.; Wang, S.; Sun, H.; Ang, H.; Tadé, M., Adsorption and heterogeneous advanced oxidation of phenolic contaminants using Fe loaded mesoporous SBA-15 and H_2O_2. *Chem. Eng. J.* **2010**, *164*, 255-260, DOI: 10.1016/j.cej.2010.08.061.

[19] Thu, P.; Dieu, H.; Phi, H.; Viet, N.; Kim, S.; Vo, V., Synthesis, characterization and phenol adsorption of carbonyl-functionalized mesoporous silicas. *J. Porous Mater.* **2012**, *19*, 295-300, DOI: 10.1007/s10934-011-9475-8.

[20] Kao, H.; Liao, C.; Palani, A.; Liao, Y., One-pot synthesis of ordered and stable cubic mesoporous silica SBA-1 functionalized with amino functional groups. *Microporous Mesoporous Mater.* **2008**, *113*, 212-223, DOI: 10.1016/j.micromeso.2007.11.030.

[21] Anbia, M.; Hariri, S., Removal of methylene blue from aqueous solution using nanoporous SBA-3. *Desalination* **2010**, *261*, 61-66, DOI: 10.1016/j.desal.2010.05.030.

[22] Da'na, E.; Sayari, A., Adsorption of heavy metals on amine-functionalized SBA-15 prepared by Co-condensation: Applications to real water samples. *Desalination* **2012**, *285*, 62-67, DOI: 10.1016/j.desal.2011.09.034.

[23] Kleitz, F.; Czuryszkiewicz, T.; Solovyov, L.; Lindén, M., X-ray structural modeling and gas adsorption analysis of cagelike SBA-16 silica mesophases prepared in a F127/Butanol/H_2O System. *Chem. Mater.* **2006**, *18*, 5070-5079, DOI: 10.1021/cm061534n.

[24] Lee, C.; Liu, S.; Juang, L.; Wang, C.; Lin, K.; Lyu, M., Application of MCM-41 for dyes removal from wastewater. *J. Hazard. Mater.* **2007**, *147*, 997-1005, DOI: 10.1016/j.jhazmat.2007.01.130.

[25] De la Iglesia, O.; Pedernera, M.; Mallada. R.; Linc, Z.; Rocha, J.; Coronas, J.; Santamaria, J., Synthesis and characterization of MCM-48 tubular membranes.

J. Hazard. Mater. **2006**, *280*, 867-875, DOI: 10.1016/j.memsci.2006.03.016.

[26] Punyapalakul, P.; Takizawa, S., Selective adsorption of nonionic surfactant on hexagonal mesoporous silicates (HMSs) in the presence of ionic dyes. *Water Res.* **2006**, *40*, 3177-3184, DOI: 10.1016/j.watres.2006.07.008.

[27] Zhao, A.; Samanta, A.; Sarkar, P.; Gupta, R., Carbon dioxide adsorption on amine-impregnated mesoporous SBA-15 sorbents: Experimental and kinetics study. *Ind. Eng. Chem. Res.* **2013**, *52*, 6480-6491, DOI: 10.1016/j.watres.2006.07.008.

[28] Kamarudin, K. S. N.; Alias, N., Adsorption performance of MCM-41 impregnated with amine for CO_2 removal. *Fuel Process. Technol.* **2013**, *106*, 332-337, DOI: 10.1016/j.fuproc.2012.08.017.

[29] Gil, M.; Tiscornia, I.; de la Iglesia, O.; Mallada, R.; Santamaria, J., Monoamine-grafted MCM-48: An efficient material for CO_2 removal at low partial pressures. *Chem. Eng. J.* **2011**, *175*, 291-297, DOI: 10.1016/j.cej.2011.09.107.

[30] Sanz, R.; Calleja, G.; Arencibia, A.; Sanz-Pe´rez, E. S., CO_2 Adsorption on branched polyethyleneimine-impregnated mesoporous silica SBA-15. *Appl. Surf. Sci.* **2010**, *256*, 5323-5328, DOI: 10.1016/j.apsusc.2009.12.070.

[31] Bhagiyalakshmi, M.; Yun, L.; Anuradha, R.; Jang, H., Utilization of rice husk ash as silica source for the synthesis of mesoporous silicas and their application to CO_2 adsorption through TREN/TEPA grafting. *J. Hazard. Mater.* **2010**, *175*, 928-938, DOI: 10.1016/j.jhazmat.2009.10.097.

[32] Ballav, N.; Maity, A.; Mishra, S. B., High efficient removal of Chromium(VI) using glycine doped polypyrrole adsorbent from aqueous solution. *Chem. Eng. J.* **2012**, *198-199*, 536-546, DOI: 10.1016/j.cej.2012.05.110.

[33] Daraei, P.; Madaeni, S. S.; Ghaemi, N.; Salehi, E.; Khadivi, M.; Moradian, R.; Astinchap, B., Novel polyethersulfone nanocomposite membrane prepared by PANI/Fe_3O_4 nanoparticles with enhanced performance for Cu(II) removal from water. *J. Membr. Sci.* **2012**, *415-416*, 250-259, DOI: 10.1016/j.memsci.2012.05.007.

[34] Ansari, R.; Mosayebzadeh, Z., Removal of basic dye methylene blue from aqueous solutions using Sawdust and sawdust coated with polypyrrole. *J. Iran. Chem. Soc.* **2010**, *7*, 339-350, DOI: 10.1007/BF03246019.

[35] Bhaumik, M.; Maity, A.; Srinivasu, V. V.; Onyango, M. S., Removal of hexavalent chromium from aqueous solution Using polypyrrole-polyaniline nanofibers. *Chem. J.* **2012**, *181-182*, 323-333, DOI: 10.1016/j.cej.2011.11.088.

[36] Mansour, M. S.; Ossman, M. E.; Farag, H. A., Removal of Cd(II) ion from waste water by adsorption onto polyaniline coated on sawdust. *Desalination* **2011**, *272*, 301-305, DOI: 10.1016/j.desal.2011.01.037.

[37] Krishnani, K. K.; Srinives, S.; Mohapatra, B. C.; Bod, V. M.; Hao, J.; Meng, X.; Mulchandani, A., Hexavalent chromium removal mechanism using conducting polymers. *J. Hazard. Mater.* **2013**, *252-253*, 99-106, DOI: 10.1016/j.jhazmat.2013.01.079.

[38] Shafiabadi, M.; Dashti, A.; Tayebi, H., Removal of Hg(II) from aqueous solution using Polypyrrole/SBA-15 nanocomposite: Experimental and modeling. *Synth. Met.* **2016**, *212*, 154-160, DOI: 10.1016/j.synthmet.2015.12.020.

[39] Tayebi, H.; Dalirandeh, Z.; Shokuhirad, A.; Mirabi, A.; Binaeian, E., Synthesis of polyaniline/Fe_3O_4 magnetic nanoparticles for removal of reactive red 198 from textile waste water: Kinetic, isotherm, And thermodynamic studies. *Desalination Water Treat.* **2016**, 1-13, DOI: 10.1080/19443994.2015.1133323.

[40] Bakala, P.; Briot, E.; Salles, L.; Bre´geault, J., Comparison of liquid-phase olefin epoxidation over MoOx inserted within mesoporous silica (MCM-41, SBA-15) and grafted onto silica. *Appl. Catal., A* **2006**, *300*, 91-99, DOI: 10.1016/j.apcata.2005.09.038.

[41] Li, Q.; Yu, H.; Song, J.; Pan, X.; Liu, J.; Wang, Y.; Tang, L., Synthesis of SBA-15/polyaniline mesoporous composite for removal of resorcinol from

aqueous solution. *Appl. Surf. Sci.* **2014**, *290*, 260-266, DOI: 10.1016/j.apsusc.2013.11.065.

[42] Katiyar, A.; Ji, L.; Smirniotis, P.; Pinto, N. G., Protein adsorption on the mesoporous molecular sieve silicate SBA-15: Effects of pH and pore size. *J. Chromatogr., A* **2005**; *1069*, 119-126. DOI: 10.1016/j.chroma.2004.10.077.

[43] Ullah, R.; Atilhan, M.; Aparicio, S.; Canlier, A.; Yavuz, C. T., Insights of CO_2 adsorption performance of amine impregnated mesoporous silica (SBA-15) at wide range pressure and temperature conditions. *Int. J. Greenh. Gas Control* **2015**, *43*, 22-32, DOI: 10.1016/j.ijggc.2015.09.013.

[44] Bui, T.; Choi, H., Adsorptive removal of selected pharmaceuticals by mesoporous silica SBA-15. *J. Hazard. Mater.* **2009**, *168*, 602-608, DOI: 10.1016/j.jhazmat.2009.02.072.

[45] Yiu, H. H. P.; Wright, P. A.; Botting, N. P., Enzyme immobilisation using SBA-15 mesoporous molecular sieves with functionalised surfaces. *J. Mol. Catal. B: Enzym.* **2001**, *15*, 81-92, DOI: 10.1016/S1381-1177(01)00011-X.

[46] Mureseanu, M.; Reiss, A.; Stefanescu, I.; David, E.; Parvulescu, V.; Renard, G.; Hulea, V., Modified SBA-15 mesoporous silica for heavy metal ions remediation. *Chemosphere* 2008, *73*, 1499-1504, DOI: 10.1016/j.chemosphere.2008.07.039.

[47] Wu, C., Adsorption of reactive dye onto carbon nanotubes: Equilibrium, kinetics and thermodynamics. *J. Hazard. Mater.* **2007**, *144*, 93-100, DOI: 10.1016/j.jhazmat.2006.09.083

[48] Kumar, P. S.; Ramalingam, S.; Senthamarai, C., Niranjanaa, M.; Vijayalakshmi, P.; Sivanesan, S., Adsorption of dye from aqueous solution by cashew nut Shell: Studies on equilibrium isotherm, kinetics and thermodynamics of interactions. *Desalination* **2010**, *261*, 52-60, DOI: 10.1016/j.desal.2010.05.032.

[49] Indra, D. M.; Vimal, C. S.; Nitin, K. A., Removal of orange-G and methyl violet dyes by adsorption onto bagasse fly ashdkinetic study and equilibrium isotherm analyses. *Dyes Pigm.* **2006**, *69*, 210-223, DOI: 10.1016/j.dyepig.2005.03.013.

[50] Peng, X.; Huang, D.; Odoom-Wubah, T.; Fu, D.; Huang, J.; Qin, Q., Adsorption of anionic and cationic dyes on ferromagnetic ordered mesoporous carbon from aqueous solution: Equilibrium, thermodynamic and kinetics. *J. Colloid. Interface. Sci.* **2014**, *430*, 272-282, DOI: 10.1016/j.jcis.2014.05.035.

[51] Aghajani, K.; Tayebi, H. A., Adaptive neuro-fuzzy inference system analysis on adsorption studies of reactive red 198 from aqueous solution by SBA-15/CTAB composite. *Spectrochim. Acta, Part A* **2017**, *171*, 439-448, DOI: 10.1016/j.saa.2016.08.025.

[52] Zhu, Z.; Li, W., Efficient adsorption and desorption of Pb^{2+} from aqueous solution. *J. Environ. Chem. Eng.* **2013**, *1*, 838-84, DOI: 10.1016/j.jece.2013.07.022.

[53] Foo, K. Y.; Hameed, B. H., Insights into the modeling of adsorption isotherm systems. *Chem. Eng. J.* **2010**, *156*, 2-10, DOI: 10.1016/j.cej.2009.09.013.

[54] Cheung, W. H.; Szeto, Y. S.; McKay, G., Intraparticle diffusion processes during acid dye adsorption onto chitosan. *Bioresour. Technol.* **2007**, *98*, 2897-2904, DOI: 10.1016/j.biortech.2006.09.045.

[55] Choy, K. K. H.; Porter, J. F.; Mckay, G., Intraparticle diffusion in single and multicomponent acid dye adsorption from wastewater onto carbon. *Chem. Eng. J.* **2004**, *103*, 133-145, DOI: 10.1016/j.cej.2004.05.012.

[56] Tsai, W. T.; Chang, C. Y.; Lin, M. C.; Chien, S. F.; Sun, H. F.; Hsieh, M. F., Adsorption of acid dye onto activated carbons prepared from agricultural waste bagasse by $ZnCl_2$ activation. *Chemosphere*. **2001**, *45*, 51-58, DOI: 10.1016/S0045-6535(01)00016-9.

[57] Sivaraj, R.; Namasivayam, C.; Kadirvelu, K., Orange peel as an adsorbent in the removal of acid violet 17 (acid dye) from aqueous solutions. *Waste. Manage.* **2001**, *21*, 105-110, DOI: 10.1016/S0956-053X(00)00076-3.

[58] Valix, M.; Cheung, W. H.; McKay, G., Preparation of activated carbon using low temperature carbonisation and physical activation of high ash raw bagasse for acid dye adsorption. *Chemosphere*.

2004, *56*, 493-501, DOI: 10.1016/ j.chemosphere.2004.04.004.

[59] Hameed, B. H.; Ahmad, A. A.; Aziz, N., Isotherms, kinetics and thermodynamics of acid dye adsorption on activated palm ash. *Chem. Eng. J.* **2007**, *133*, 195-203, DOI: 10.1016/j.cej.2007.01.032.

[60] Konicki, W.; Sibera, D.; Mijowska, E.; Lendzion-Bielun, Z.; Narkiewicz, U., Equilibrium and kinetic studies on acid dye acid red 88 adsorption by magnetic $ZnFe_2O_4$ spinel ferrite nanoparticles J. *Colloid. Interface. Sci.* **2013**, *398*, 152-160, DOI: 10.1016/j.jcis.2013.02.021.

[61] Akar, S. T.; Uysal, R., Untreated clay with high adsorption capacity for effective removal of C.I. Acid red 88 from aqueous solutions: Batch and dynamic - flow mode studies. *Chem. Eng. J.* **2010**, *162*, 591598, DOI: 10.1016/j.cej.2010.06.001.

[62] Özcan, A. S.; Erdem, B.; Özcan, A., Adsorption of acid blue 193 from aqueous solutions onto Na-bentonite and DTMA-bentonite. *J. Colloid. Interface. Sci.* **2004**, *280*, 44-54, DOI: 10.1016/ j.jcis.2004.07.035.

[63] Arami, M.; Limaee, N. Y.; Mahmoodia, N. M.; Tabrizi, N. S., Equilibrium and kinetics studies for the adsorption of direct and acid dyes from aqueous solution by soy meal hull. *J. Hazard. Mater.* **2006**, *B135*, 171-179, DOI: 10.1016/j.jhazmat.2005.11.044.